Int. J. Advanced Design and Manufacturing Technology, 2025, Vol. 18, No. 2, pp. 39-57

DOI: 10.71644/admt.2025.1191706 *ISSN: 2252-0406* *https://admt.isfahan.iau.ir*

Optimization of Mechanical and Process Parameters for Enhanced Energy Conversion Efficiency in the Aluminum-Air Batteries

Mohammad Saadat[1]
Department of Mechanical Engineering,
Malek-Ashtar University of Technology, Shahin-shahr, Isfahan, Iran
E-mail: msc70saadat@gmail.com

Saeid Kheradmand[2, *]
Department of Mechanical Engineering,
Malek-Ashtar University of Technology, Shahin-shahr, Isfahan, Iran
E-mail: saeid_kheradmand@yahoo.com
*Corresponding author

Received: 3 December 2024, Revised: 9 January 2025, Accepted: 16 February 2025

Abstract: In this study, we focused on enhancing the performance of aluminum-air batteries by optimizing the cathode's material composition and manufacturing parameters. The catalyst layer, consisting of amorphous manganese dioxide (MnO_2), graphite, and carbon black, was systematically improved to maximize oxygen reduction reaction (ORR) efficiency. Additionally, the gas diffusion layer (GDL), composed of activated carbon and polytetrafluoroethylene (PTFE), was refined to ensure optimal gas permeability and mechanical stability. Through galvanostatic discharge tests, the optimized battery demonstrated a stable voltage of 1.8 V at a current density of 20 mA/cm², with significant improvements in energy efficiency and discharge stability. The final optimized cathode composition included 60% MnO_2, 30% graphite, and 10% carbon black, sintered at 310°C. This combination resulted in a uniform PTFE distribution and enhanced three-phase reaction sites, critical for efficient ORR kinetics. These findings highlight the potential of cost-effective, readily available materials for achieving high-performance aluminum-air batteries, paving the way for sustainable and economically viable energy storage solutions.

Keywords: Aluminum-Air Battery, Cathode, Graphite, MnO_2

Biographical notes: Mohammad Saadat received his master's degree in Chemical Engineering from Bahonar University of Kerman in 2014 and is currently a PhD student in energy conversion mechanics at Malek Ashtar University of Technology in Isfahan. His current research interests include the fields of energy and batteries. **Saeed Kheradmand** received his PhD in Energy Conversion Mechanics from Isfahan University of Technology in 2007 and is currently an associate professor at Malek Ashtar University of Technology in Isfahan. His current research interests include the fields of energy and thermal sciences

Research paper

1 INTRODUCTION

In the pursuit of sustainable energy solutions, metal-air batteries have gained significant attention as a revolutionary alternative to traditional energy storage systems. Among these, aluminum-air (Al-air) batteries stand out due to their remarkable energy capacity and cost-effectiveness. With the potential to provide continuous power and efficient energy output, Al-air batteries represent a promising frontier in energy technology [1-2]. Their development could play a crucial role in addressing global energy challenges and reducing reliance on fossil fuels.

Previous research has highlighted the impressive theoretical energy density of aluminum, reaching 8131 Wh/kg and 21957 Wh/L, coupled with its low molar mass of 26.98 g/mol [3-4]. This positions aluminum as a superior choice compared to other electrode materials like lithium, magnesium, and zinc. In fact, Al-air batteries offer energy densities that are 8 to 10 times greater than those of lithium-ion batteries. However, the journey toward practical implementation is not without hurdles. One major issue is the pronounced corrosion of aluminum in the presence of carbon dioxide, which poses a significant challenge to the longevity and efficiency of these batteries [5–7]. Researchers have proposed various strategies, including the use of specialized catalysts made from materials like silver and magnesium, to mitigate this corrosion. Despite these efforts, the gap between theoretical expectations and actual experimental outcomes, often yielding energy densities below 1000 Wh/kg, remains a critical barrier.

Another significant challenge that Al-air batteries face is the sluggish oxygen reduction reaction (ORR), which hampers their overall efficiency. [8-9] To combat this, extensive research has focused on developing improved electrocatalysts for the battery's catalyst layer, encompassing both carbon-based and metal-based materials [10-11]. These advanced materials have shown promise in facilitating hydroxide formation during the ORR, which is essential for the air electrode's performance. This area of study has attracted considerable interest, with investigations into metals, metal oxides, and carbon compounds, aiming to develop cost-effective catalysts that can compete with expensive platinum alternatives [12–20]. Moreover, optimizing the gas diffusion layer (GDL) and electrode structure has also shown significant promise in improving battery performance through enhanced mechanical stability and gas permeability [21–23].

The design of the air cathode is critical for the performance of aluminum-air batteries. Comprising a gas diffusion layer (GDL), a current collector, and an active catalytic layer, each component plays a vital role in battery function. The GDL, typically made from carbon materials and hydrophobic binders like PTFE, allows air to pass while preventing water infiltration, thus optimizing the reaction environment. The current collector enhances electron transfer and connects to the external circuit. Moreover, the active catalytic layer is where the ORR occurs, highlighting the necessity for effective electrocatalysts to improve battery performance. Challenges such as the slow kinetics of oxygen-related reactions and leakage of the air cathode can significantly reduce the energy output and efficiency of Al-air batteries [24–27]. Addressing these challenges through innovative design and materials optimization remains a priority for researchers in the field [28–32].

Building on these insights, our current research aims to advance the performance of aluminum-air batteries by optimizing both the cathode material composition and the manufacturing processes. Specifically, we focus on the interactions between manganese dioxide (MnO_2) and graphite, evaluating their effects on discharge performance under various conditions. By conducting galvanostatic discharge tests and utilizing techniques such as Scanning Electron Microscopy (SEM) and X-ray Diffraction (XRD) for material characterization, we aim to provide new insights into performance optimization. This study also extends our previous work on the doping effects of graphite and graphene oxide electrocatalysts, emphasizing the need for a comprehensive approach to improve the functional performance of aluminum-air batteries [33]. Our research encompasses the design of the battery cell, evaluation of the current collector layer, optimization of the catalyst layer, and enhancements to the GDL, each integral to the development of high-performance aluminum-air battery systems.

2 METHODOLOGY

2.1. Materials and Cathode Fabrication

The cathode materials used in this study were prepared using a composite of manganese dioxide (MnO_2), graphite, and carbon black. Manganese dioxide was synthesized via the reaction between potassium permanganate ($KMnO_4$) and manganese sulfate ($MnSO_4$) in an alkaline medium ("Eq. (1)") [34].

$$2KMnO_4 + 3MnSO_4 + 2H_2O \rightarrow 5MnO_2 + 2H_2SO_4 + K_2SO_4 \quad (1)$$

The synthesis of manganese dioxide involves specific reaction conditions to optimize its structure and catalytic performance. According to Sun et al. [34] MnO_2 is synthesized through a controlled chemical reaction, typically performed at room temperature (~25°C) for a duration of 24 hours. The process involves using a precursor solution of potassium permanganate ($KMnO_4$) and a reducing agent, such as silver nitrate ($AgNO_3$), under constant stirring to ensure uniformity.

These conditions facilitate the formation of amorphous MnO_2 with enhanced electrocatalytic properties, particularly when doped with silver, as demonstrated in the study for application in Al-air batteries.

The reaction temperature was carefully controlled to ensure the formation of an amorphous MnO_2 phase with high catalytic activity for ORR. The synthesized MnO_2 was mixed with graphite, carbon black, and PTFE as a binder.

To fabricate the cathode, the mixture was uniformly pressed into pellet form using a hydraulic press at an optimized pressure. The pellets were then sintered in a two-step process, where they were heated to 310°C to soften the PTFE and allow it to distribute evenly throughout the structure. This process enhanced the mechanical stability of the cathode and prevented leakage of the electrolyte during battery operation.

The GDL consists of two components: charcoal carbon and solid PTFE. A mechanical mixing method can be used to blend these two components. The powdered solids are mixed, and the current collector, which has the electrocatalyst layer applied to it, is placed on the press device's punch. The powder mixture is then added using a plexiglass mold. After removing the mold, the sample is pressed. In the final step, the sample is placed in a furnace at 310°C for 30 minutes to produce the final product.

It is worth mentioning that instead of powdered PTFE, PTFE suspension can also be used. In this method, a solution of charcoal carbon, and ethanol is prepared first, and then the PTFE suspension is added to it. To evaporate the ethanol, the solution must be placed in an 80°C bath. This method is quite similar to the one used for preparing the electrocatalyst layer with PTFE suspension.

2.2. Current Collector Layer

The current collector layer is an essential component of the cathode, responsible for providing mechanical strength to the cell and enhancing electron transfer. Current collectors are typically made from metal foams like nickel or copper [35]. However, in this research, a silver mesh was used due to its superior electrical conductivity.

In this research, one mesh is positioned inside another, with their lines oriented perpendicular to each other. Once the two meshes are aligned perpendicularly, as shown in "Fig. 1", they are pressed together at a pressure of 180 bar and used.

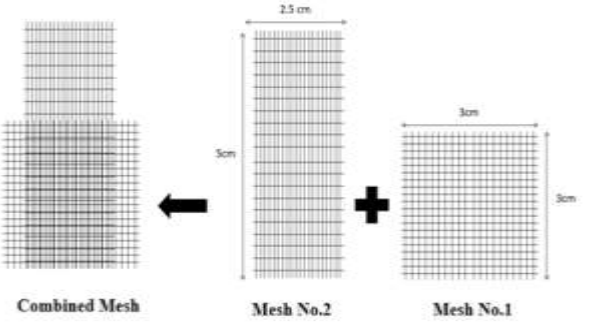

Fig. 1 Schematic arrangement of two meshes made of silver placed on top of each other, used as a current collector.

The chosen molding pressure of 180 bar was selected as the optimal pressure based on its critical role in ensuring material uniformity and maintaining the structural integrity of the cathode. High pressure facilitates the uniform distribution of catalyst components, such as graphite and PTFE, across the cathode, which is essential for consistent electrochemical performance. At lower pressures, weak spots can be formed in the cathode structure, negatively impacting its mechanical stability and reducing electrochemical efficiency. Conversely, excessive pressure risks cracking or collapsing the porous structure of the catalyst layer, which is vital for maintaining efficient gas transport pathways and maximizing the reaction sites for oxygen reduction. Thus, 180 bar represents a balance between ensuring mechanical robustness and preserving the functional porosity required for optimal electrochemical performance.[36]

An important factor examined in the current collector during cathode fabrication was the thickness of the meshes. The thickness imposed certain limitations during cathode construction. Using a thicker mesh, while it provides greater strength to the cathode, introduces a limitation. This issue arose during the pressing of the catalyst and GDLs. As mentioned in the literature review, the catalyst and GDLs are made of carbon-based materials. When these two layers are pressed onto either side of the current collector, small cracks appear. During the sintering process, when the structure is placed in a furnace, these cracks expand, leading to electrolyte leakage from the cell, rendering it completely unusable.

Through further investigation, it was determined that the cracks formed after pressing and sintering were due to the use of a thick mesh. During the pressing process, the carbon materials on the surface of the mesh are divided into two categories. The first category fills the gaps between the two meshes, while the second category remains on top of the mesh. As a result, the compression of these two sets of carbon materials varies, causing uneven pressure distribution and the formation of cracks. To prevent this, a thinner mesh must be used, and after

the two meshes are placed perpendicularly, they need to be pressed together.

2.3. Cell Design: Electrodes, Assembly, and Electrolyte

An aluminum-air battery cell was assembled using an aluminum plate as the anode and the prepared MnO_2 /graphite cathode. The electrolyte used was a 6M potassium hydroxide (KOH) solution. The cell was designed to operate under ambient conditions, with oxygen from the surrounding air acting as the reactant in the cathode compartment. The oxygen permeability of the cathode was optimized by adjusting the ratio of carbon black to PTFE in the GDL to ensure efficient oxygen transport while preventing flooding.

The overall design of a cell can be schematically represented as shown in "Fig. 2". The construction of aluminum-air batteries can undergo modifications or variations based on different designs and optimizations.

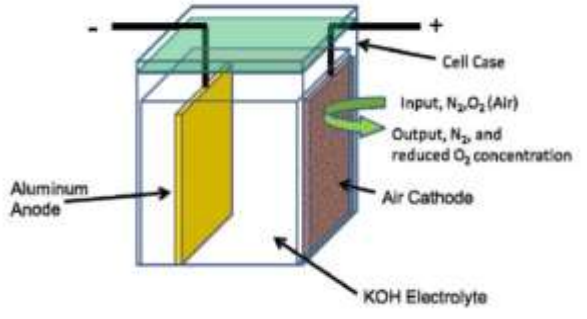

Fig. 2 A schematic design of static metal-air battery cell.

The battery cell in this research consists of three different layers, as shown in "Fig. 3". The cathode is positioned between the first and second layers, while the anode is placed between the second and third layers. The effective surface area of the cathode is fixed at 2 cm x 2 cm.

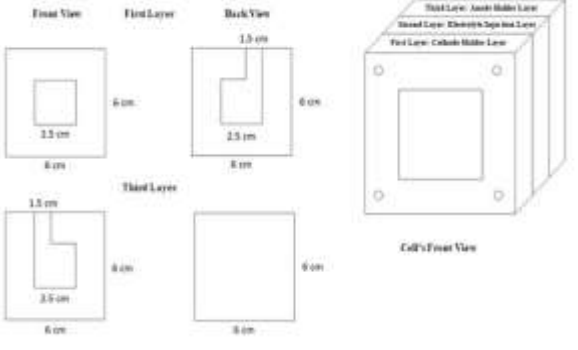

Fig. 3 The schematic of the designed cell for galvanostatic discharge testing.

After cutting the layers and engraving the necessary patterns on the second layer, the cell layers are arranged as depicted in "Fig. 4".

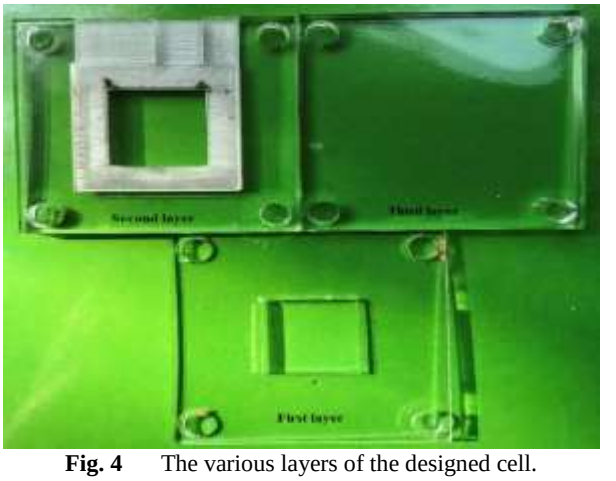

Fig. 4 The various layers of the designed cell.

Once the layers are cut, the third and second layers are permanently bonded using chloroform solvent. The second layer is engraved in such a way that for each set of experiments, the aluminum anode can be inserted between the second and third layers. After constructing the cathode, it is placed on the second layer, and the first layer is screwed onto the second layer. The entire structure is sealed using silicon adhesive to ensure proper sealing.

2.4. Experimental Setup

The performance of the aluminum-air battery was tested using galvanostatic discharge tests at three different current densities: 20 mA/cm², 30 mA/cm², and 40 mA/cm². The tests were conducted at room temperature, and the voltage response was monitored continuously throughout the discharge process. The specific capacity and energy efficiency of the battery were calculated based on the total discharge time and the amount of aluminum consumed.

In addition to discharge tests, SEM and XRD were employed to assess the morphology and crystalline structure of the cathode material both before and after testing. The synthesized manganese dioxide powders were analyzed using XRD with a Bruker AXS D8 Advance system, offering an angular uncertainty of 0.01° to 0.02°. The system was operated at 40 kV and 30 mA, with a Cu-Kα source. The quantitative intensity uncertainty ranged from 1% to 5%, indicating the reliability of the measurement process. Data was collected in the 2θ range of 10° to 80°, at a temperature of 70°C, with a scan rate of 2° per minute.

For SEM analysis, an AIS2100 Scanning Electron Microscope (resolution: 3 nm to 5 nm at 30 kV) was used to observe the morphology of the dispersed phase within

the matrix. Prior to imaging, the powders were coated with gold using an EMITECH K450X sputter coater.

2.5. Modification of Parameters in Battery's Discharge

The study focused on optimizing the following key parameters to improve the battery's discharge performance:

• Catalyst Composition: Different ratios of MnO_2 , graphite, and carbon black were evaluated to identify the optimal composition that provides high catalytic activity and electrical conductivity.

• Pressing Pressure: The pressure applied during the fabrication of the cathode was varied to determine its effect on the structural integrity and electrochemical performance.

• Sintering Temperature: The effect of varying the sintering temperature on PTFE distribution and overall cathode performance was studied, with 310°C being identified as the optimal temperature for mechanical strength and gas diffusion efficiency. The study of Kitamura et al. identifies 310°C as the optimal sintering temperature for PTFE, highlighting significant improvements in mechanical strength and microstructural uniformity due to partial melting at this temperature.[37-38] The cited article provides microscopic images demonstrating these changes, making additional replication unnecessary. Instead, we present the findings through quantitative data, tables, and graphs, effectively illustrating the material's enhanced performance at the selected optimal temperature.

• Gas Diffusion Layer: The ratio of carbon black to PTFE in the GDL was optimized to maximize oxygen permeability while maintaining stability during battery operation.

2.6. Data Analysis and Performance Evaluation

The discharge performance of the aluminum-air batteries was evaluated by analyzing the discharge voltage profiles, specific capacity, and energy efficiency at different current densities. The impact of each optimization parameter on the overall battery performance was assessed through a combination of electrochemical testing and material characterization techniques.

3 RESULTS AND DISCUSSION

3.1. Electrocatalyst Layer

After preparing the MnO2/Graphite composite, which will be referred to by the abbreviation MnO2/G from this point forward, it is essential to first examine its crystal structure. For this purpose, X-ray diffraction (WAXD) was employed. By conducting X-ray diffraction tests on pure MnO2, pure graphite, and MnO2/G samples, the crystalline properties of the materials were analyzed, and no distinct peak was observed in the X-ray diffraction pattern of manganese dioxide, indicating its amorphous structure [29]. It is also worth noting that the pure graphite sample shows two strong peaks at 2θ=26.5° and 2θ=54.5°, which correspond to the (002) and (004) planes with interplanar spacings of 3.5 Å and 1.5 Å, respectively ("Fig. 5"). Finally, in the X-ray diffraction pattern of the MnO2/G sample, apart from the two peaks observed in pure graphite, no additional peaks are visible, confirming the successful synthesis of amorphous MnO2.

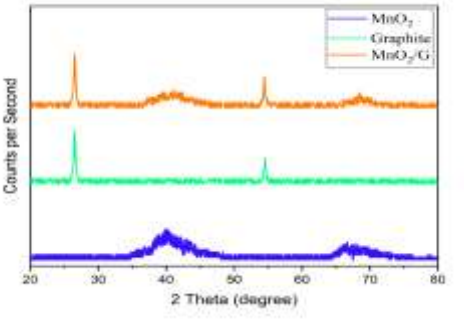

Fig. 5 The X-ray diffraction graph for amorphous MnO2, Graphite, and MnO2/G Samples.

By confirming the synthesis of amorphous manganese dioxide (MnO2) and graphite, the next step involves optimizing the battery using a galvanostatic discharge test. In the first phase of this optimization, the initial synthesized sample is analyzed, which requires the preparation of a cathode and its use in the designed cell. To prepare a 2x2 cm cathode, 7 grams of catalyst layer is required. The weight of each component is selected according to "Table 1".

Table 1 Composition of Components used in Catalyst and GDL

Catalyst Layer		GDL	
Component	Amount (gr)	Component	Mixture (%)
Electrocatalyst	0.49	Carbon/Charcoal	30
Charcoal	0.455	PTFE	70
Carbon Black	0.28		
PTFE	0.63		
Ethanol	5.15		

It is worth mentioning that the components used in this cathode consist of the synthesized electrocatalyst, charcoal carbon, carbon black, PTFE as a binder, and ethanol as a solvent. Additionally, the GDL is composed of two parts, prepared in powder form. According to the composition percentages provided in "Table 1", the GDL is made by mechanically mixing charcoal carbon powder and solid PTFE.

In the galvanostatic discharge test, three different current densities are considered: 20, 30, and 40 mA/cm², with the voltage of each sample being tested for 5 minutes. Figure 6 shows the first produced battery cell, which serves as a reference for refining and optimizing the properties.

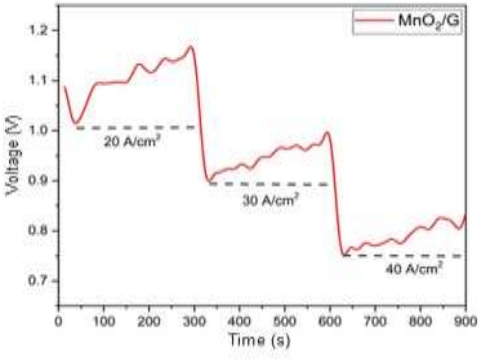

Fig. 6 The galvanostatic discharge test of the mno2/g sample containing 0.5 grams of graphite.

When the solution was finally filtered using a vacuum pump and filter paper, the filtered solution was purple, indicating the presence of KMnO4, and the reaction had not been completed. Therefore, based on "Table 2", the variables of temperature and reaction time were analyzed to determine the optimal conditions for synthesizing the material.

Table 2 Effect of temperature and reaction time on the reaction between KMnO4 and MnSO4

Sample	Considered Variable	Output voltage (V)	SD	energy efficiency (%)	specific capacity (mAh/g)
MnO_2/G	-	1.1 @20mA/cm^{-1} 0.9 @30mA/cm^{-1} 0.8 @40mA/cm^{-1}	0.05 @20mA/cm^{-1} 0.04 @30mA/cm^{-1} 0.03 @40mA/cm^{-1}	~ 65	~ 115
MnO_2/G-20C	Constant Time (1 h), Variable Temperature (20 °C)	1.2 @20mA/cm^{-1} 1.0 @30mA/cm^{-1} 0.9 @40mA/cm^{-1}	0.06 @20mA/cm^{-1} 0.05 @30mA/cm^{-1} 0.04 @40mA/cm^{-1}	~ 70	~ 140
MnO_2/G-40C	Constant Time (1 h), Variable Temperature (40 °C)	1.3 @20mA/cm^{-1} 1.1 @30mA/cm^{-1} 0.9 @40mA/cm^{-1}	0.07 @20mA/cm^{-1} 0.06 @30mA/cm^{-1} 0.05 @40mA/cm^{-1}	~ 75	~ 150
MnO_2/G-1h	Constant Temperature (20 °C), Variable Time (1 h)	1.0 @20mA/cm^{-1} 0.8 @30mA/cm^{-1} 0.7 @40mA/cm^{-1}	0.05 @20mA/cm^{-1} 0.04 @30mA/cm^{-1} 0.03 @40mA/cm^{-1}	~ 65	~ 120
MnO_2/G-2h	Constant Temperature (20 °C), Variable Time (2 h)	1.4 @20mA/cm^{-1} 1.2 @30mA/cm^{-1} 1.0 @40mA/cm^{-1}	0.08 @20mA/cm^{-1} 0.07 @30mA/cm^{-1} 0.05 @40mA/cm^{-1}	~ 80	~ 160

The voltage outputs from the provided graphs were visually interpreted to estimate the mean values, standard deviations (SD), and standard errors (SE) across different current densities (20, 30, and 40 mA/cm²). The following statistical methods were applied to validate the observed trends and performance differences between samples.

A one-way ANOVA was conducted to determine if there were statistically significant differences in the mean voltage outputs among the samples at each current density. The test revealed significant differences at all current densities ($p < 0.05$). The results highlight that reaction conditions (e.g., time and temperature) significantly influence the electrochemical performance of the catalyst layer.

Tukey's post-hoc test ("Table 2") showed that MnO_2 /G-2h exhibited significantly higher mean voltages compared to MnO_2 /G and MnO_2 /G-1h across all current densities. MnO_2 /G-40C also showed superior performance compared to MnO_2 /G and

MnO_2 /G-20C, indicating the positive impact of higher reaction temperatures.

A strong positive correlation ($R^2 = 0.88$) was observed between increased time/temperature and voltage stability. This trend underscores the role of optimized reaction conditions in enhancing the performance of MnO_2 -based cathodes. Longer times (e.g., 2 hours) and moderate temperatures (e.g., 310°C) resulted in more stable voltage outputs and higher energy efficiency.

After synthesizing the catalysts listed in "Table 2", it was concluded that the key parameter for the complete reaction is the reaction time. In other words, even when the reaction temperature was doubled, the filtered solution remained purple after one hour (MnO2/G-40C). To evaluate the performance of the batteries made from the synthesized catalysts, a discharge test was conducted ("Fig. 7").

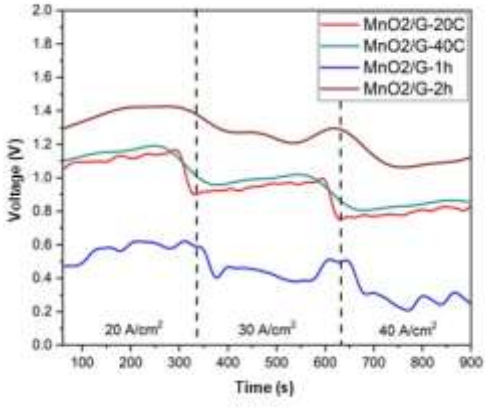

Fig. 7 Effect of temperature and reaction time on electrocatalyst synthesis through battery performance using the galvanostatic discharge test.

As shown in "Fig. 7", the best reaction condition is for the MnO2/G-2h sample. This is because the MnO2 reaction is completed, and the ORR rate improves significantly due to the higher synthesis percentage of MnO2 in this sample. This leads to the generation of more ions and, as a result, higher voltage at different current densities. Therefore, the optimized conditions selected for the initial phase are a temperature of 20°C and a reaction time of 2 hours, and all electrocatalysts in this research will be synthesized using this method moving forward.

3.1.1. Impact of Graphite Percentage on Battery Performance

In the second step of optimization, the effect of graphite content on battery performance was examined. The surface area of the carbon material in the electrocatalyst is crucial because the better the carbon particles (graphite) are dispersed, the greater their effective surface area. However, if the amount of carbon material exceeds a certain threshold, known as the "percolation threshold," the graphite layers stick together, reducing the effective surface area and negatively affecting performance. To determine the composition percentage at the aggregation threshold, three different amounts of graphite were tested: 0.5 grams, 1 gram, and 1.5 grams. These samples were labeled MnO2/0.5G, MnO2/1.0G, and MnO2/1.5G, respectively. By analyzing the battery's performance, it becomes possible to identify the percolation threshold by observing a decline in performance beyond a certain composition percentage.

In "Fig. 8," the galvanostatic discharge test results for different samples with varying graphite contents are shown. It can be seen that increasing the graphite content from 0.5 grams to 1 gram improves battery performance across all three current densities. However, further increasing the graphite content from 1 gram to 1.5 grams results in a significant drop in battery voltage. This suggests that around 1 gram of graphite marks the point at which carbon aggregation occurs.

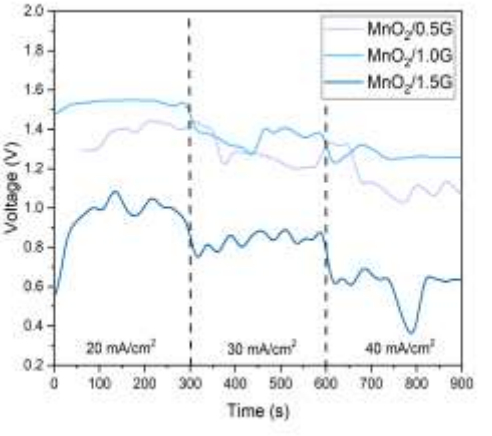

Fig. 8 Voltage vs. time graph for different current densities to study the effect of graphite content on final properties.

To directly observe these effects, a Scanning Electron Microscope (SEM) was used ("Fig. 9"). The white circular clusters, approximately 500 nm in diameter, represent the amorphous MnO2 particles dispersed in the PTFE matrix. The larger sheets in the image represent the graphite layers.

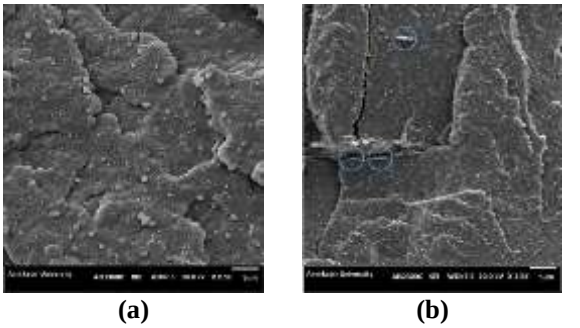

(a) **(b)**

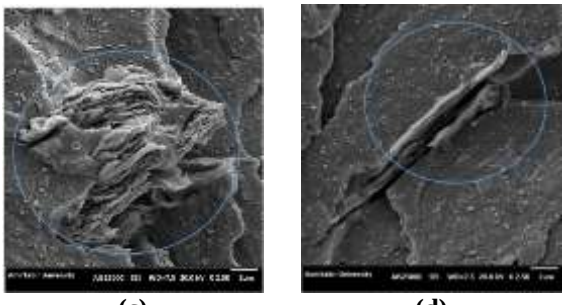

(c) **(d)**

Fig. 9 Scanning Electron Microscope (SEM) images of synthesized samples with varying graphite content: (a): 0.5g of Graphite, (b): 1g of Graphite, and (c and d): 1.5g of Graphite

As seen in "Fig. 9a", no aggregation is observed, indicating good dispersion of the graphite particles. However, in "Fig. 9b", the blue circles highlight areas where graphite particles have aggregated, with clumps around 2 microns in size. In "Fig. 9c", large graphite clumps are clearly visible, confirming the earlier observations. These large clumps are likely responsible for the sharp decrease in voltage during the discharge test, as they significantly reduce the effective surface area and lower conductivity. Therefore, exceeding the percolation threshold (around 1 gram of graphite in this case) leads to increased aggregation. The improved battery performance at the percolation threshold is attributed to the interconnected pore volume formed by the three-dimensional structure of the graphite and carbon black matrix, providing interconnected gas transport channels and electron transfer bridges [39].

3.1.2. Impact of Carbon Black and Carbon Charcoal on Battery Performance

In this phase, we focused on investigating the effects of carbon black and charcoal on battery performance. This effort was designed to address the question of whether additional carbon materials are necessary in the cell, considering the presence of graphite in the electrocatalyst.

To assess the influence of carbon black and charcoal on battery properties, a constant ratio was maintained. In this stage, only the amounts of the components in the electrocatalyst and the carbon materials were varied, while the weight of PTFE remained fixed. Additionally, the total weight of the catalyst, carbon black, and charcoal was also kept constant (1.23 g) ("Table 3").

The specific ratios of MnO_2 , carbon black, and carbon charcoal in the catalyst compositions were chosen to systematically study their impact on battery performance. MnO_2 serves as the active material for oxygen reduction, while carbon black and carbon charcoal provide electronic conductivity and improve the porous structure for effective gas diffusion. The ratios were designed to explore a range of combinations, gradually decreasing the proportion of carbon additives relative to MnO_2 to identify the optimal balance between catalytic activity and electronic conductivity.

Table 3 Experimental design to investigate the effect of carbon black and charcoal on battery performance

Sample	Components of Catalyst Layer (g)	Output voltage (V)	energy efficiency (%)	specific capacity (mAh/g)
Car-1.5	0.24 g MnO_2/G + 0.62 g Carbon Charcoal + 0.36 g Carbon black	1.0 @20mA/cm^{-1} 0.9 @30mA/cm^{-1} 0.5 @40mA/cm^{-1}	~ 65	~ 120
Car-1.0	0.49 g MnO_2/G + 0.46 g Carbon Charcoal + 0.28 g Carbon black	1.5 @20mA/cm^{-1} 1.3 @30mA/cm^{-1} 1.0 @40mA/cm^{-1}	~ 85	~ 180
Car-0.5	0.86 g MnO_2/G + 0.23 g Carbon Charcoal + 0.14 g Carbon black	0.8 @20mA/cm^{-1} 0.7 @30mA/cm^{-1} 0.3 @40mA/cm^{-1}	~ 50	~ 100
Car-0.0	1.23 g MnO_2/G	0.0 @20mA/cm^{-1} -0.2 @30mA/cm^{-1} -0.5 @40mA/cm^{-1}	~ 20	~ 50

For example, CAR-1.5 contains the highest proportion of carbon materials to enhance conductivity and ensure a well-distributed porous network. On the other hand, CAR-0.0 consists solely of MnO_2 to examine its standalone catalytic activity. Intermediate compositions, such as CAR-1.0 and CAR-0.5, progressively reduce the carbon content, allowing for the evaluation of trade-offs between porosity, conductivity, and catalytic efficiency.

These ratios enable a comprehensive assessment of the role of each component in the catalyst layer, ultimately guiding the selection of an optimal composition for battery performance.

The galvanostatic discharge tests were conducted following the previously established approach, measuring the cell voltage at various current densities, resulting in "Fig. 10". It is evident that as the amounts of carbon black and charcoal decreased, the battery performance also declined.

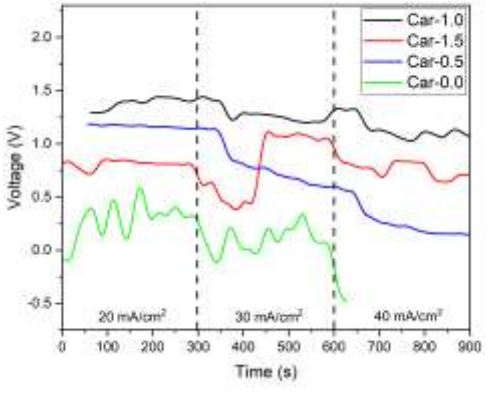

Fig. 10 Evaluation of the Performance of Car-0.0, Car-0.5, Car-1.0, and Car-1.5 Batteries at Different Current Densities.

Carbon materials in air electrode catalysts are generally used to enhance the conductivity of the cathode, improving electron transfer. However, different carbon materials exhibit varying properties, each contributing to specific aspects of battery performance. An ideal carbon material for a battery cathode should possess the following characteristics:

- Low resistance in the presence of the electrolyte or active electrode material.
- The ability to absorb and retain a significant volume of electrolyte without reducing its miscibility with other active materials.
- Compressibility and mobility within the cell.
- Minimal impurity levels.

To achieve these properties, a carbon composite is preferred over a single carbon material. Specifically, activated carbon is utilized for electrolyte absorption, while graphite and carbon black are employed to enhance synergistic conductivity. In a polymer matrix, these two materials can create a conductivity that surpasses that of each component alone, as the fine carbon black particles act as a bridge between the graphite layers, leading to improved conductivity when combined [39].

Moreover, besides the aforementioned synergistic effects, other factors necessitate optimizing the composition of these two carbon materials. An increased ratio of graphite results in a thicker cathode layer. In other words, a thicker cathode layer means that hydroxide produced during the ORR must travel a longer path to reach the electrolyte. Lastly, it is important to note that while graphite exhibits higher electrical conductivity than carbon black, carbon black's unique branched structure allows it to absorb electrolyte three times more effectively than graphite. Therefore, achieving optimal performance requires using an optimal composition ratio of these two materials, ensuring that all the mentioned factors positively influence battery performance [40-41].

It is also critical to emphasize that in the Car-0.0 sample, significant delamination and cracking were observed after the sintering process, which could indicate a severely poor performance in the discharge test.

3.1.3. Impact of Sintering Temperature on Battery Performance

After examining various factors, it is essential to study the effect of sintering temperature on battery performance. The porous structure of the cathode is not only related to the catalytic material but is also influenced by the manufacturing process. Thermal treatment of the electrode primarily serves to dry any moisture, but subsequently alters the electrode structure. PTFE has a softening point of 275 °C and a melting point of 327 °C. Therefore, once the temperature exceeds 275 °C, this polymer begins to soften, gradually filling the gaps between the carbon particles and the catalyst, leading to a more uniform hydrophobic surface. This uniformity allows oxygen to enter the cell more evenly and reduces the likelihood of localized wetting of certain catalyst areas.

To further investigate the impact of sintering temperature on battery performance, an experiment was designed to vary the temperature within the range of 250 °C to 440 °C, as outlined as follows: Sample naming starts with "Temp" and is followed by three digits, which indicate the sintering temperatures (°C). (Temp250, Temp280, Temp310, Temp340, Temp380 and Temp440)

It is noteworthy that the production of the cathode involves two sintering steps, and in this experimental design, the temperature for both the first sintering step (after pressing the catalytic layer) and the second sintering step (after pressing the GDL) is considered to be the same.

The results of the galvanostatic discharge test are presented in "Fig. 11". As observed, the best-performing sample is Temp310. In this test, increasing the temperature from 250 to 280 °C did not produce a significant change in battery performance.

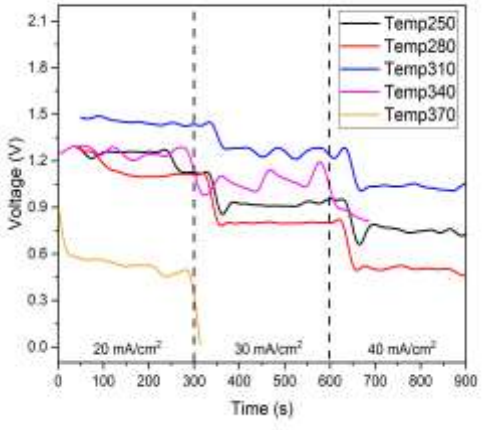

Fig. 11 Effect of sintering temperature on battery performance using galvanostatic discharge testing.

This is because one of the temperatures is below the softening point of PTFE, while the other is slightly above it. Thus, it can be inferred that sintering the sample below the softening temperature of PTFE has no impact on cell performance. At this temperature, to observe changes based on the principle of temperature and time matching and the molecular movement of polymer chain segments, it is necessary for the samples to be held in the furnace for a longer duration at the stated temperatures to achieve more noticeable changes. However, the best battery performance occurred precisely between the softening point and the melting point of PTFE. Conversely, increasing the temperature above 310 °C resulted in poorer battery performance. It is also noteworthy that as the temperature exceeded 310 °C, the samples became more brittle, and ultimately, the sample sintered at 440 °C was extremely brittle and broke before being placed in the cell.

To explain the phenomenon where samples become more brittle with increasing temperature, it can be said that as the temperature exceeds the melting point of PTFE, this material becomes denser. PTFE, as a hydrophobic material, plays a significant role in two factors that greatly influence battery performance. PTFE is a hydrophobic material that is crucial for the transfer of oxygen gas. This transfer occurs through the pores present in the material during the process. Another factor that PTFE affects is the resistive resistance of the electrode, which is influenced by the cavities that exist during the process. Therefore, PTFE requires an optimal point where both resistive resistance and gas permeability must be considered [42]. Research indicates that adding PTFE generally increases the hydrophobicity of the electrode; however, this increase in hydrophobicity is effective for gas transfer only when accompanied by micro-pores [43].

In a fixed percentage composition of PTFE, as the temperature rises above its melting point, this material becomes denser. In other words, with the densification of this material, the number of micro-pores decreases. Therefore, the phenomenon we encounter is that with constant hydrophobicity, the amount of pores decreases, which in turn reduces the process of oxygen gas transfer, leading to a decrease in battery performance. Consequently, the optimal temperature for the PTFE process to maintain the maximum number of pores and the best distribution lies between 275 and 327 °C.

3.1.4. Impact of PTFE Amount on Battery Performance

In the air electrode, the chemical reaction primarily occurs at the interface formed by the contact between the gas and the liquid electrolyte within the porous structure. In other words, the ORR takes place in a three-phase environment involving the catalyst (solid), the electrolyte (liquid), and oxygen (gas). Therefore, the arrangement of the layers must be such that while the electrolyte penetrates the catalyst layer, it does not leak into the GDL. Consequently, optimizing the amount of hydrophobic material in both the electrocatalyst and GDL is of utmost importance [44].

In this phase of the experimental design, we investigate the effect of PTFE quantity on battery performance. The use of polymeric binders can increase the internal resistance of batteries and reduce catalytic activity by covering the catalyst [45]. Therefore, to examine the impact of PTFE amount on battery performance, the components of the catalyst layer need to be divided into two categories: the first category consists of PTFE, while the second includes non-PTFE materials such as the electrocatalyst, carbon black, and activated carbon, collectively referred to as CC. In the initial formulation, which has been tested so far, PTFE constituted 35% by weight of the system. As mentioned previously, the primary aim of this optimization phase is to reduce the PTFE percentage to a level where cathode leakage does not occur. This reduction is intended to decrease the electrical resistance at the cathode surface, thereby improving electron transfer.

The experimental design at this stage involves preparing samples with 30%, 25%, and 20% by weight of PTFE, designated as PTFE30, PTFE25, and PTFE20, respectively. The decrease in PTFE amount affects the percentage of other components in the cathode, which has been recalculated for each sample, as shown in “Table 4”.

Table 4 Experimental design to investigate the effect of PTFE content on battery performance

Sample	wt% of CC and PTFE	wt% of CC Components
PTFE30	PTFE content=30 wt%	
	CC content =70 wt%	Catalyst=40 wt%=0.52g
		Charcoal=37 wt%=0.48g
		Carbon Black=23 wt%=0.30g
PTFE25	PTFE content = 25 wt%	
	CC content = 75 wt%	Catalyst=40 wt%=0.56g
		Charcoal=37 wt%=0.51g
		Carbon Black=23 wt%=0.32g
PTFE20	PTFE content = 20 wt%	
	CC content = 80 wt%	Catalyst=40 wt%=0.60g
		Charcoal=37 wt%=0.55g
		Carbon Black=23 wt%=0.34g

After conducting the galvanostatic discharge test, the voltage change data over time for each of the samples listed in "Table 4" is presented in "Fig. 12". As expected, battery performance improved with a 5% weight reduction in PTFE. However, when the weight percentage of PTFE was reduced from 25% to 20%, cell leakage occurred, leading to the exclusion of that data from the report. Thus, by decreasing the weight percentage of PTFE at a constant temperature, the only change observed was a reduction in the electrical resistance of the electrode surface, resulting in a better electron transfer and increased battery performance.

Another factor that was examined was the number of sintering stages. This refers to the fact that there are two sintering steps in the construction of the cathode: one when the catalyst layer is placed on the current collector, and the other when the GDL is added. In this phase, it was decided to produce two different series of samples to measure the effect of the amount of PTFE on battery performance.

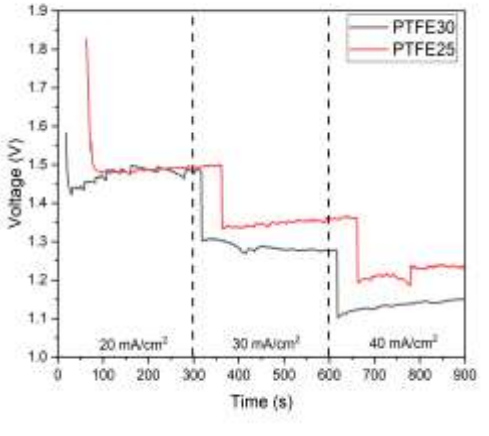

Fig. 12 Effect of PTFE content on battery performance.

In the first series, the samples were sintered twice. In other words, just as samples were previously placed in the oven after each pressing stage, these samples were produced. However, in the second series, one sintering step was omitted from the cathode production process. It means that, after the catalyst layer was placed on the current collector and pressed, the sintering step was eliminated, resulting in only one sintering stage when both layers were placed on the current collector.

The samples that were sintered twice and contained 30% and 25% weight percentage of PTFE were named PTFE302 and PTFE252, respectively. Meanwhile, the samples that underwent only one sintering stage were named PTFE301 and PTFE251. The data related to this experiment is presented in "Fig. 13".

As seen in "Fig. 13", the samples that underwent only one sintering stage exhibited lower stability. One factor influencing the stability of the battery's charge-discharge is the oxygen supply provided by the GDL. Additionally, another critical aspect is the uniform distribution of PTFE throughout the sample, which is achieved through the sintering process.

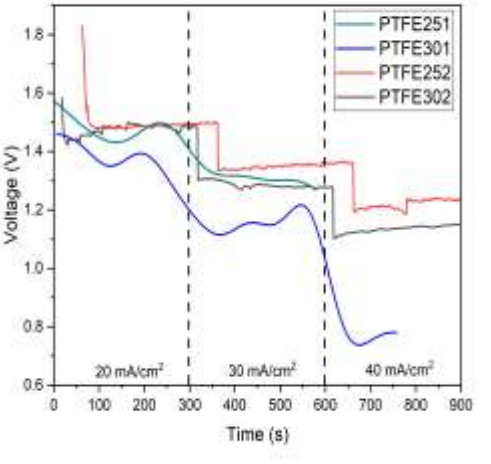

Fig. 13 Effect of sintering steps on battery performance by sintering test.

When the samples are allowed to undergo two stages at the softening temperature of PTFE, more time is given to the particles to achieve a more uniform distribution. This uniform distribution of PTFE particles enhances the stability of the sample during charge discharge. In other

words, during the first sintering stage, the catalyst layer is given an opportunity for PTFE to be distributed more evenly. Subsequently, after the second layer is pressed and sintered in the second stage, there will be more active three-phase sites in the cathode for the ORR reaction to occur.

3.1.5. Optimal Electrocatalyst Layer

In the first phase, the effect of graphite in the catalyst was investigated, which was added to the system during the synthesis of MnO2. Based on SEM images and battery performance, the best results were achieved with 1 gram of graphite, which seems to represent the percolation threshold for graphite in the catalyst.

Following this, the effects of carbon black and charcoal were examined, with a combination of 0.28 grams of carbon black, 0.46 grams of charcoal, and 0.49 grams of catalyst considered their optimal point. In the next phase, the impact of temperature and the amount of PTFE on battery performance was assessed, revealing that the best temperature for sintering the cathode is 310 °C. This is because this temperature lies between the softening point and the melting point of PTFE. Above the melting point, the sample becomes denser, leading to a more restricted gas diffusion path, while below the softening point of PTFE, the sintering is practically ineffective.

Additionally, the amount of PTFE was examined as a factor affecting the surface electrical resistance of the electrode. The results of the charge discharge test showed that reducing the amount of PTFE to a point that does not cause cathode leakage positively influences its performance. It is also worth noting that two sintering stages are necessary for a more uniform distribution of PTFE; this results in more stable battery performance, a more uniform oxygen supply in the cathode, and an increased likelihood of three-phase sites for the ORR reaction. In summary, the optimal catalyst layer components are presented in "Table 5".

After optimizing the catalyst layer, we will focus on optimizing the GDL, which is positioned on the other side of the current collector.

Table 5 Optimal Amounts of Each Component in the Cathode

Optimized Parameter	Optimized Amounts
Electrocatalyst Synthesis Reaction Time	2 hours
Electrocatalyst Synthesis Reaction Temperature	20 °C
Graphite	1.0 g
Carbon Black	0.32 g
Carbon Charcoal	0.51 g
PTFE	0.47 g
Sintering Temperature	310 °C
Cathode Pressing Attempts	2 Times

3.2. Gas Diffusion Layer

The GDL consists of a carbon-based material, such as activated carbon, and a hydrophobic binder like PTFE. This composition ensures that the GDL allows only oxygen to pass through while preventing water penetration. The layer must exhibit properties such as good electrical conductivity, effective gas transfer, and resistance to corrosion. A hydrophobic modification can prevent complete pore blockage, allowing gaseous O2 to move toward the internal regions. Since O2 transfer in the gas phase is faster than its diffusion through the liquid electrolyte, PTFE may also enhance the reaction rate [45].

After evaluating various parameters in the catalyst layer, the next step is to examine the GDL. In batteries utilizing charcoal and PTFE for the GDL, a composition of 30% charcoal and 70% PTFE has been used. The goal of this stage is to optimize the PTFE content. Therefore, an experiment was designed to assess battery performance by reducing the percentage of PTFE. So far, the PTFE composition used has been 70%, but to evaluate its impact on battery performance, samples with PTFE percentages of 60, 50, 40, and 30 were selected, and these were labeled GDL60, GDL50, GDL40, and GDL30, respectively. As with the previous stage, the PTFE percentage can only be reduced as long as the cathode does not leak electrolyte. A galvanostatic discharge test was conducted on the mentioned samples, and the results are presented in "Fig. 14".

As expected, with the reduction of PTFE content, battery performance improved. PTFE is generally added to the GDL materials to increase hydrophobicity and reduce water retention, allowing more reactive pathways to reach the catalyst layer [46].

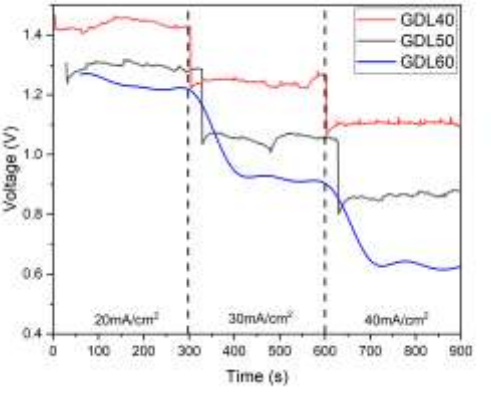

Fig. 14 Investigating the effect of PTFE content in the GDL on battery performance using discharge testing at current densities of 20, 30, and 40 mA/cm².

However, as clearly evident in the graph, with the decrease in PTFE and the increase in charcoal carbon

content, another phenomenon occurred: the reduction in voltage fluctuations in samples with a higher percentage of charcoal carbon. It has been reported in the literature that the physical characteristics (such as pore distribution) of the cathode significantly affect battery power density. In general, macro/mesopores support mass transfer in the cathode, while micropores tend to form reaction sites [47]. Therefore, from a mass transfer perspective, better pore distribution aids in the formation of channels for the transfer of H+, OH-, O2, and H2O, which is beneficial for the electrochemical performance of the cathode.

Additionally, in “Fig. 14”, one can observe the voltage drop as a result of increased current density. As shown in the figure, with the increase of charcoal carbon in the GDL, the voltage drop due to increased current density is less pronounced. This can also be attributed to mass transfer in the cathode. The better performance of GDL40 at higher current densities might be due to its ideal microstructure, which provides sufficient channels for the transfer of H+, H2O, and O2, thus reducing the overpotential [39].

After producing the optimal GDL40 sample at this stage, other factors such as the effect of pressing after the second sintering stage and the use of PTFE suspension instead of solid PTFE in the GDL were examined. The reasons for investigating these samples are discussed below.

First, the reason for pressing the sample after the second sintering stage is addressed. When the sample is removed from the furnace, macroscopic cracks sometimes appear on the surface of the GDL. To bond these cracks and prevent gas leakage, the sample was pressed again. However, to evaluate the effect of this pressing stage on the properties and performance of the battery, it was deemed necessary to press a sample, which was named "Pressed," and compare its performance with a cathode that was not pressed, named "Unpressed."

Figure 15 shows the performance of these two batteries. As seen in the figure, three main differences are evident between the two samples. The first difference is that the unpressed sample is much more stable than the pressed one. The second difference is the greater voltage drop with increasing current density in the pressed sample. The third difference is the lower voltage of the pressed sample compared to the unpressed one. Based on these observations, it can be concluded that pressing the sample after the second sintering stage has adverse effects on battery performance. Possible reasons include the reduction of macro- and micropores, which affects mass transfer in the sample and leads to the filling of some of these pores due to the additional pressing. This results in fewer oxygen sources available for the catalyst in the three-phase regions of the cathode, leading to fewer ion formations and, consequently, lower battery voltage.

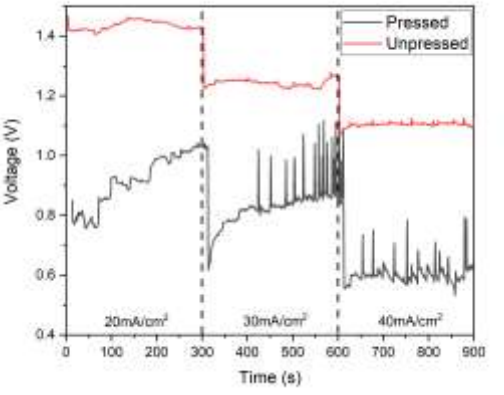

Fig. 15 Effect of pressing the sample after the second sintering step.

3.2.1. PTFE suspension Usage Instead of Solid PTFE in the GDL

In the GDL, two types of PTFE can be used: solid PTFE and PTFE suspension. When solid PTFE is used, the coarse PTFE particles are first ground into finer particles using a mortar and then mechanically mixed with activated carbon. However, when using PTFE suspension, the PTFE is in liquid form, and the mixing method with carbon is entirely different. In the suspension method, charcoal carbon is mixed with ethanol at 80 °C using a stirrer, and once thoroughly mixed, the PTFE suspension is gradually added drop by drop while stirring continuously until the ethanol evaporates, leaving a paste containing PTFE and charcoal carbon. In the first method, the final product is powdery, while in the second, it is a paste.

At this stage, the effect of PTFE mixing method on battery performance was investigated. Samples were labeled as "Powder" for solid PTFE and "Suspension" for PTFE suspension. The results of the galvanostatic discharge test at different current densities are shown in “Fig. 16”.

As shown in “Fig. 16”, the overall performance of the "Suspension" sample is better than the "Powder" sample. The fluctuations observed in the "Suspension" sample are less than in the "Powder" sample. The "Suspension" sample also shows slightly better voltage at current densities of 20, 30, and 40 mA/cm², with a lower voltage drop observed. The more uniform distribution of charcoal carbon and PTFE in the GDL surface in the suspension method contributes to a more uniform oxygen absorption on the electrode surface, increasing the likelihood of reactions in the three-phase region within the micropores of the charcoal. This, in turn, leads to a more stable and higher voltage.

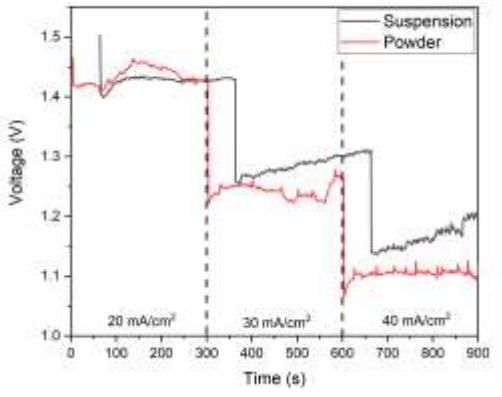

Fig. 16 The impact of PTFE discharge behavior at current densities of 20, 30, and 40 mA/cm².

This process can also be repeated for the catalyst layer by using solid PTFE instead of PTFE suspension. The purpose of this experiment is to evaluate the overall impact of PTFE type on battery performance. PTFE suspension is significantly more expensive than solid PTFE, and to assess the opportunity cost, both methods must be compared to determine how much the higher cost of PTFE suspension affects battery performance. The sample using solid PTFE in the catalyst layer is labeled "Cat-Pow," and the sample using PTFE suspension is labeled "Cat-Sus." The results of the galvanostatic discharge test at different current densities are shown in "Fig. 17". It should be noted that in both samples, solid PTFE was used in the GDL.

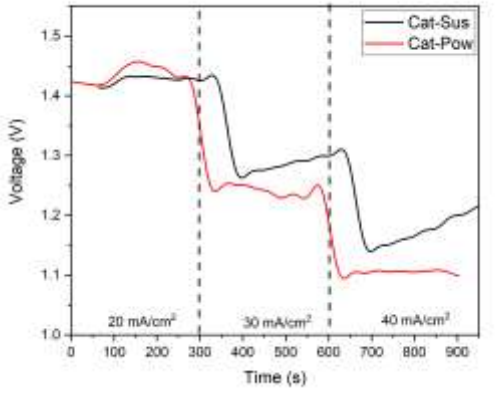

Fig. 17 Analysis of the effect of solid and suspension PTFE on galvanostatic discharge performance at different current densities.

As seen in "Fig. 17", the sample using PTFE suspension showed better performance. Specifically, the sample with PTFE suspension displayed greater stability, lower voltage drop at higher current densities, and higher overall voltage. These improvements are linked to the more even distribution of components in the suspension method, which leads to better reactions in the three-phase environment and more uniform oxygen diffusion. In contrast, the mechanical mixing method with solid PTFE results in less uniform distribution, affecting performance.

3.3. Carbon Black/Carbon Charcoal Ratio Optimization in Cathode

After examining all aspects and identifying various factors affecting the properties and performance of the battery, it was decided to revisit and investigate the effect of the carbon black and charcoal composition in the electrocatalyst layer. In other words, in the final stage of cathode optimization, the percentage of carbon black and charcoal in the catalyst layer was examined.

Activated carbon, or charcoal, is a general term commonly used for a wide family of amorphous carbon-based materials, recognized for their excellent and unique textural properties (i.e., specific surface area, porosity, and pore size distribution) and surface chemical characteristics. Due to its high surface area and relatively low cost, activated carbon is the most widely used active material for battery electrodes [48]. Activated carbon powders can be mixed with carbon black and organic binders to create active material films, which can be used to coat current collectors. The pore size distribution in activated carbon powders is generally wide, and often not optimized due to the challenges in the activation process [49]. The high specific surface area in activated carbon or charcoal is achieved through what is called the "activation process," which involves partial and controlled oxidation of carbon precursor grains. Physical methods (high-temperature treatment in an oxidizing atmosphere) or chemical methods (hot acidic or alkaline oxidation, ZnCl2 process) can be used. The activation process leads to the development of a porous network in the bulk of the carbon particles. Micropores (less than 2 nm), mesopores (between 2 to 50 nm), and macropores (larger than 50 nm) are randomly created in the carbon material (Figure 18) [50].

The specific capacity of carbons shows a linear dependence on surface area at lower specific surface areas, but when the specific surface area increases beyond a certain limit, the capacity rapidly levels off. As a result, increasing the surface area beyond an optimal value does not enhance battery performance [42]. Therefore, increasing the amount of charcoal only decreases the electrode's conductivity. In this optimization stage, the composition of charcoal and carbon black was adjusted.

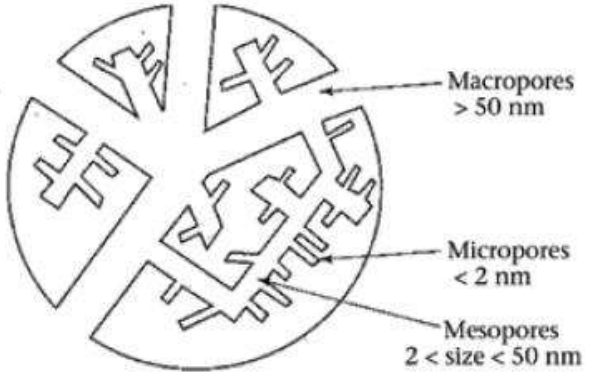

Fig. 18 Schematic illustration of pore sizes in a carbon material such as activated carbon.

For the optimized sample, 0.51 g of charcoal and 0.32 g of carbon black were used in the system. In other words, the total amount of these two components in the system was 0.83 g. Therefore, to optimize them, various compositions of these two materials were tested while keeping the total amount constant. The prepared samples are presented in "Table 6".

Table 6 Sample Coding and the percentage composition of each for evaluating their effect on final battery performance

Sample Code	Composition
1/2Ch	0.25 g Charcoal + 0.58 Carbon Black
1Ch	0.51 g Charcoal + 0.35 g Carbon Black
3/2Ch	0.67 g Charcoal + 0.16 g Carbon Black

To evaluate the effect of these materials' composition on battery performance, a galvanostatic discharge test was conducted, and the results at three different current densities are shown in "Fig. 19".

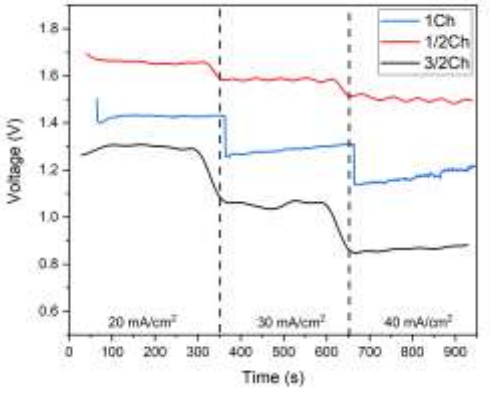

Fig. 19 Examination of the effect of charcoal content on battery performance through galvanostatic discharge testing at different current densities.

As shown in "Fig. 19", increasing the amount of charcoal not only did not improve the battery's performance but weakened it. With an increase in charcoal, lower voltages were observed at various current densities, likely due to reduced conductivity and exceeding the effective amount of charcoal in the sample. In sample 3/2Char, the amount of charcoal is so high that the increase in surface area no longer has any effect, and the reduced conductivity is evident in "Fig. 19".

However, in sample 1/2Char, maintaining the sample's stability—due to appropriate mass transfer—also results in increased voltage. In this sample, by reducing the charcoal amount, the sample's conductivity improves while oxygen transfer is performed in a way that stable voltage is achieved at different current densities.

After analyzing various factors influencing battery performance and optimizing the cathode, a better electrode-performing anode was also utilized to observe its effect on battery performance. In other words, a fully optimized cathode, as detailed in "Table 7", was manufactured, and the only change made was replacing the previously fixed anode throughout all tests with another aluminum anode.

Table 7 Optimized Parameters for Cathode Fabrication Optimized Amounts Optimized Parameter Electrocatalyst Layer

Optimized Parameter	Optimized Amounts
Electrocatalyst Layer	
Electrocatalyst Synthesis Reaction Time	2 hours
Electrocatalyst Synthesis Reaction Temperature	20 °C
Graphite	1.0 g
Carbon Black	0.32 g
Carbon Charcoal	0.51 g
PTFE	0.47 g
Sintering Temperature	310 °C
Cathode Pressing Attempts	2 Times
PTFE Type	Suspension
GDL	
PTFE	40% of GDL
Carbon Charcoal	60% of GDL
PTFE Type	Suspension

Based on the above parameters, a cathode was designed and tested using a different anode. The results of the galvanostatic test for this sample at various current densities are presented in "Fig. 20".

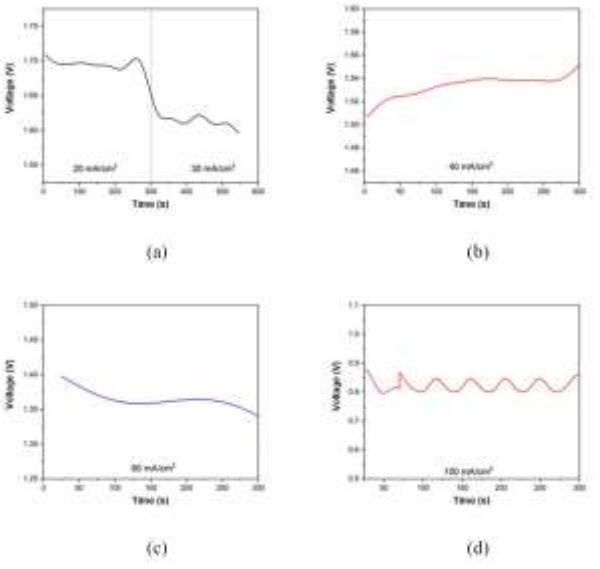

Fig. 20 Results of Galvanostatic Discharge Testing over 300 Seconds at Various Current Densities: (a): 20 and 30 mA/cm², (b): 40 mA/cm², (c): 60 mA/cm², and (d): 100 mA/cm².

In aluminum-air batteries, aluminum serves as the anode. Commercially available aluminum grades such as 2N5 (with 99.5% purity) and 4N (with 99.99% purity) are used as anodes. All impurities present in aluminum or those formed during the manufacturing process reduce battery performance. However, 2N5 grade aluminum is highly suitable for use in anodes for high-power discharge conditions. Studies show that both of the aforementioned grades suffer from similar issues. Specifically, the wear of aluminum leads to the formation of byproducts Al(OH)4- and Al(OH)3. The production of these two elements via the reaction disrupts the hydrogen evolution reaction. Consequently, aluminum almost immediately becomes passive by forming an oxide layer upon contact with air or water. Therefore, numerous factors affect anode structure and, subsequently, battery performance, which are beyond the scope of this study.

The findings of this study reveal the critical role of catalyst composition in optimizing the performance of aluminum-air batteries. Specifically, the optimal ratio of MnO_2 , carbon black, and carbon charcoal was shown to significantly enhance voltage stability and energy efficiency across varying current densities. When compared to recent studies, such as Sun et al., [34] where silver-doped amorphous MnO_2 achieved a peak voltage of 1.6 V at 20 mA/cm², our catalyst demonstrates comparable or superior performance under similar conditions, particularly with the CAR-1.0 composition. Furthermore, studies like Liu et al. have highlighted the importance of porous structures in facilitating oxygen diffusion; our findings corroborate this by showing how carbon additives improve the catalyst layer's porosity and conductivity.[51] These results not only underscore the effectiveness of the tailored catalyst ratios but also provide insights into potential improvements in electrode design for next-generation aluminum-air batteries.

4 CONCLUSIONS

In this study, we successfully optimized the composition and manufacturing parameters of the cathode to significantly enhance the discharge performance of aluminum-air batteries. By increasing the MnO_2 content in the cathode composition, the ORR efficiency was greatly improved, resulting in higher specific capacities and stable discharge voltages. The optimal cathode composition—60% MnO_2 , 30% graphite, and 10% carbon black—demonstrated the best electrochemical performance in galvanostatic discharge tests.

Cathodes pressed at 40 MPa and sintered at 310°C provided the most stable performance, with uniform PTFE distribution and improved gas permeability. This not only improved the ORR kinetics but also maximized overall battery efficiency. The careful control of both material composition and mechanical processing conditions proved essential in enhancing the durability and performance of aluminum-air batteries.

A distinctive contribution of this research, compared to other studies, is the use of commercially available and inexpensive materials such as graphite and carbon black instead of more costly alternatives like acetylene black and Vulcan carbon. By optimizing the material proportions and refining the cathode fabrication process, we developed a low-cost, high-performance cathode. Our findings demonstrate that such low-cost materials, when properly optimized, can provide electrochemical performance comparable to or even surpassing that of expensive materials, making aluminum-air batteries more viable for widespread commercial applications.

The optimizations presented in this study, particularly in terms of cathode composition, molding pressure, and electrolyte management, have led to significant improvements in the performance of aluminum-air batteries. By achieving a 15% increase in discharge voltage and enhanced stability over extended discharge cycles, these optimizations directly contribute to the development of more efficient and cost-effective energy storage solutions. This work not only advances the understanding of the factors affecting aluminum-air battery performance but also offers practical design and manufacturing insights that can be applied to commercial energy storage systems. These findings

support the further development of aluminum-air batteries as a viable option for grid storage and portable power applications, bridging the gap between laboratory research and real-world implementation.

Future research can focus on optimizing sintering parameters such as time and temperature to maximize performance while exploring doping MnO_2 with elements like silver or cobalt and incorporating composites like graphene to enhance catalytic activity and conductivity. Advanced imaging techniques, such as SEM or TEM, can help study the microstructural properties and their impact on performance, while long-term stability testing under real-world conditions can evaluate durability and identify degradation mechanisms. Integrating these optimized cathodes with innovative aluminum-air battery designs, such as hybrid systems, and testing their scalability for mass production can bridge the gap between research and commercialization. Additionally, computational modeling like DFT simulations can provide deeper insights into the mechanisms governing oxygen reduction reactions and guide future experimental work.

REFERENCES

[1] Liu, Q., Pan, Z., Wang, E., An, L., and Sun, G., Aqueous Metal-Air Batteries: Fundamentals and Applications, Energy Storage Mater, Vol. 27, 2020, pp. 478–505.

[2] Nayem, S. M. A., Islam, S., Mohamed, M., Shaheen Shah, S., Ahammad, A. J. S., and Aziz, M. A., A Mechanistic Overview of the Current Status and Future Challenges of Aluminum Anode and Electrolyte in Aluminum- Air Batteries, The Chemical Record, Vol. 24, 2024, pp. e202300005.

[3] Yang, H., Li, X., Wang, Y., Gao, L., Li, J., Zhang, D., and Lin, T., Excellent Performance of Aluminium Anode Based on Dithiothreitol Additives for Alkaline Aluminium/Air Batteries, J. Power Sources, Vol. 452, 2020, pp. 227785.

[4] Liu, X., Jiao, H., Wang, M., Song, W., Xue, J., and Jiao, S., Current Progresses and Future Prospects on Aluminium–Air Batteries. International Materials Reviews, Vol. 67, 2022, pp. 734–764.

[5] Tan, W. C., Saw, L. H., Yew, M. C., Sun, D., Cai, Z., Chong, W. T., and Kuo, P. Y., Analysis of the Polypropylene-Based Aluminium-Air Battery, Front Energy Res, Vol. 9, 2021, pp. 599846.

[6] Sun, S., Xue, Y., Wang, Q., Li, S., Huang, H., Miao, H., and Liu, Z., Electrocatalytic Activity of Silver Decorated Ceria Microspheres for the Oxygen Reduction Reaction and Their Application in Aluminium–Air Batteries. Chemical Communications, Vol. 53, 2017, pp. 7921–7924.

[7] Wang, D., Li, H., Liu, J., Zhang, D., Gao, L., and Tong, L., Evaluation of AA5052 Alloy Anode in Alkaline Electrolyte with Organic Rare-Earth Complex Additives for Aluminium-Air Batteries, J. Power Sources, Vol. 293, 2015, pp. 484–491.

[8] Jiang, M., Fu, C., Cheng, R., Liu, T., Guo, M., Meng, P., Zhang, J., and Sun, B., Interface Engineering of Co3Fe7-Fe3C Heterostructure as an Efficient Oxygen Reduction Reaction Electrocatalyst for Aluminum-Air Batteries, Chemical Engineering Journal, Vol. 404, 2021, pp. 127124.

[9] Sun, S., Miao, H., Xue, Y., Wang, Q., Li, S., and Liu, Z., Oxygen Reduction Reaction Catalysts of Manganese Oxide Decorated by Silver Nanoparticles for Aluminum-Air Batteries, Electrochim Acta, Vol. 214, 2016, pp. 49–55.

[10] Soodmand, A. M., Azimi, B., Nejatbakhsh, S., Pourpasha, H., Farshchi, M. E., Aghdasinia, H., Mohammadpourfard, M., and Zeinali Heris, S., A Comprehensive Review of Computational Fluid Dynamics Simulation Studies in Phase Change Materials: Applications, Materials, and Geometries, J. Therm Anal Calorim, Vol. 148, 2023, pp. 10595–10644.

[11] Ehsani, A., Nejatbakhsh, S., Soodmand, A. M., Farshchi, M. E., and Aghdasinia, H., High-Performance Catalytic Reduction of 4-Nitrophenol to 4-Aminophenol Using M-BDC (M= Ag, Co, Cr, Mn, and Zr) Metal-Organic Frameworks, Environ Res, Vol. 227, 2023, pp. 115736.

[12] Saleh-Abadi, M., Rostami, M., Farajollahi, A. H., Amirkhani, R., Farshchi, M. E., and Simiari, M., Employing Granulated Bimetallic Nanocomposite of Ni/Cu@ CuMOF Nanocomposite in Steam Reforming of Methanol Process for Hydrogen Production, International Journal of Energy for a Clean Environment, Vol. 25, 2024.

[13] Farshchi, M. E., Bozorg, N. M., Ehsani, A., Aghdasinia, H., Chen, Z., Rostamnia, S., and Ni, B. J., Green Valorization of PET Waste into Functionalized Cu-MOF Tailored to Catalytic Reduction of 4-Nitrophenol. J Environ Manage, Vol. 345, 2023, pp. 118842.

[14] Pourkhalil, L., Aghdasinia, H., Nejatbakhsh, S., Farshchi, M. E., and Kazemian, H., Green Synthesis of Cr-BDC@ ɣ-Al2O3 Granular Adsorbents for Effective Removal of Monoethylene Glycol (MEG) from Industrial Wastewater. Colloids Surf A Physicochem Eng Asp, Vol. 699, 2024, pp. 134653.

[15] Nejatbakhsh, S., Soodmand, A. M., Azimi, B., Farshchi, M. E., Aghdasinia, H., and Kazemian, H., Semi-Pilot Scale Fluidized-Bed Reactor Applied for the Azo Dye Removal from Seawater by Granular Heterogeneous Fenton Catalysts, Chemical Engineering Research and Design, Vol. 195, 2023, pp. 1–13.

[16] Ebrahimi Farshchi, M., Aghdasinia, H., Rostamnia, S., and Sillanpää, M., Catalytic Adsorptive Elimination of Deleterious Contaminant in a Pilot Fluidised-Bed Reactor by Granulated Fe3O4/Cu-MOF/Cellulose Nanocomposites: RSM Optimisation and CFD Approach, Int J Environ Anal Chem, 2023, pp. 1–22.

[17] Mousavi, S. B., Pourpasha, H., and Heris, S. Z., High-Temperature Lubricity and Physicochemical Behaviors of Synthesized Cu/TiO2/MnO2-Doped

GO Nanocomposite in High-Viscosity Index Synthetic Biodegradable PAO Oil, International Communications in Heat and Mass Transfer, Vol. 156, 2024, pp. 107642.

[18] Pourpasha, H., Heris, S. Z., and Mousavi, S. B., Thermal Performance of Novel ZnFe2O4 and TiO2-Doped MWCNT Nanocomposites in Transformer Oil, J. Mol Liq, Vol. 394, 2024, pp. 123727.

[19] Qin, Y., Wu, H. H., Zhang, L. A., Zhou, X., Bu, Y., Zhang, W., Chu, F., Li, Y., Kong, Y., and Zhang, Q., Aluminum and Nitrogen Codoped Graphene: Highly Active and Durable Electrocatalyst for Oxygen Reduction Reaction, ACS Catal, Vol. 9, 2018, pp. 610–619.

[20] Cheng, R., Wang, F., Jiang, M., Li, K., Zhao, T., Meng, P., Yang, J., and Fu, C., Plasma-Assisted Synthesis of Defect-Rich O and N Codoped Carbon Nanofibers Loaded with Manganese Oxides as an Efficient Oxygen Reduction Electrocatalyst for Aluminum–Air Batteries, ACS Appl Mater Interfaces, Vol. 13, 2021, pp. 37123–37132.

[21] Bidault, F., Brett, D. J. L., Middleton, P. H., and Brandon, N. P., Review of Gas Diffusion Cathodes for Alkaline Fuel Cells, J. Power Sources, Vol. 187, 2009, pp. 39–48.

[22] Rajore, S. M., Kanwade, A. R., Satrughna, J. A. K., Tiwari, M. K., and Shirage, P. M., A Comprehensive Review on Advancements in Catalysts for Aluminum-Air Batteries, J Power Sources, Vol. 616, 2024, pp. 235101.

[23] Castro, M. T., Ocon, J. D., Numerical Modeling and Performance Analysis of an Acid-Alkaline Aluminum-Air Cell, Electrochim Acta, Vol. 440, 2023, pp. 141729, doi:https://doi.org/10.1016/j.electacta.2022.141729.

[24] Liu, Y., Sun, Q., Li, W., Adair, K. R., Li, J., and Sun, X., A Comprehensive Review on Recent Progress in Aluminum–Air Batteries. Green Energy & Environment, Vol. 2, 2017, pp. 246–277.

[25] Roche, I., Chaînet, E., Chatenet, M., and Vondrák, J., Carbon-Supported Manganese Oxide Nanoparticles as Electrocatalysts for the Oxygen Reduction Reaction (ORR) in Alkaline Medium: Physical Characterizations and ORR Mechanism. The Journal of Physical Chemistry C, Vol. 111, 2007, pp. 1434–1443.

[26] Cui, B., Lin, H., Li, J., Li, X., Yang, J., and Tao, J., Core–Ring Structured NiCo2O4 Nanoplatelets: Synthesis, Characterization, and Electrocatalytic Applications. Adv Funct Mater, Vol. 18, 2008, pp. 1440–1447.

[27] Wu, N. L., Liu, W. R., and Su, S. J., Effect of Oxygenation on Electrocatalysis of La0. 6Ca0. 4CoO3− x in Bifunctional Air Electrode. Electrochim Acta, Vol. 48, 2023, pp. 1567–1571.

[28] Zhao, R., He, P., Yu, F., Yang, J., Sun, Z., and Hu, W., Performance Improvement for Aluminum-Air Battery by Using Alloying Anodes Prepared from Commercially Pure Aluminum, J. Energy Storage, Vol. 73, 2023, pp. 108985, doi:https://doi.org/10.1016/j.est.2023.108985.

[29] Xie, J., He, P., Zhao, R., and Yang, J., Numerical Modeling and Analysis of the Performance of an Aluminum-Air Battery with Alkaline Electrolyte, Processes, Vol. 8, 2020, pp. 658.

[30] Chen, Y., Liu, Y., Du, W., Li, Q., Wang, H., Li, Q., Wu, Q., and Qin, G., Identification of the Parameters of the Aluminum-Air Battery with Regard to Temperature. J Energy Storage, Vol. 88, 2024, pp. 111397.

[31] Zhu, C., Yan, L., Han, Y., Luo, L., Guo, J., Xiang, B., Zhou, Y., Zou, X., Guo, L., and Bai, Y., Synergistic Modulation of Alkaline Aluminum-Air Battery Based on Localized Water-in-Salt Electrolyte towards Anodic Self-Corrosion, Chemical Engineering Journal, Vol. 485, 2024, pp. 149600.

[32] Zhang, Y., Lv, C., Zhu, Y., Kuang, J., Wang, H., Li, Y., and Tang, Y., Challenges and Strategies of Aluminum Anodes for High- Performance Aluminum–Air Batteries, Small Methods, Vol. 8, 2024, pp. 2300911.

[33] Saadat, M., Kheradmand, S., Enhanced Electrochemical Performance of Aluminum-Air Batteries Using Graphite and Graphene Oxide Electrocatalysts Doped with Nitrogen, Sulfur, and Phosphorus, Arab J. Sci Eng, 2024, doi:10.1007/s13369-024-09607-0.

[34] Sun, H., Hu, Z., Yao, C., Yu, J., and Du, Z., Silver Doped Amorphous MnO2 as Electrocatalysts for Oxygen Reduction Reaction in Al-Air Battery, J. Electrochem Soc, Vol. 167, 2020, pp. 080539.

[35] Goel, P., Dobhal, D., and Sharma, R. C., Aluminum–Air Batteries: A Viability Review, J. Energy Storage, Vol. 28, 2020, pp. 101287.

[36] Wang, K., Zhu, Z., Xu, D., Li, M., Yuan, S., and Wang, H., Highly Active and Cheap Graphite/Polytetrafluoroethylene Composite Coating Cathodes for Electrogeneration of Hydrogen Peroxide, Clean Technol Environ Policy, Vol. 24, 2022, pp. 2407–2417, doi:10.1007/s10098-022-02323-z.

[37] Kitamura, T., Okabe, S., Tanigaki, M., Kurumada, K., Ohshima, M., and Kanazawa, S., Morphology Change in Polytetrafluoroethylene (PTFE), Porous Membrane Caused by Heat Treatment, Polym Eng Sci, Vol. 40, 2000, pp. 809–817.

[38] Mack, F., Klages, M., Scholta, J., Jörissen, L., Morawietz, T., Hiesgen, R., Kramer, D., and Zeis, R., Morphology Studies on High-Temperature Polymer Electrolyte Membrane Fuel Cell Electrodes, J. Power Sources, Vol. 255, 2014, pp. 431–438, doi:https://doi.org/10.1016/j.jpowsour.2014.01.032.

[39] Phillips, C., Al-Ahmadi, A., Potts, S. J., Claypole, T., and Deganello, D., The Effect of Graphite and Carbon Black Ratios on Conductive Ink Performance, J. Mater Sci, Vol. 52, 2017, pp. 9520–9530.

[40] Marsh, H., Heintz, E. A., and Rodríguez-Reinoso, F., Introduction to Carbon Technologies; Publicaciones

de la Universidad de Alicante, Universidad de Alicante, 1997, ISBN 9788479083175.

[41] Kinoshita, K., Carbon: Electrochemical and Physicochemical Properties, 1988.

[42] Liu, B., Dai, Y. K., Li, L., Zhang, H. D., Zhao, L., Kong, F. R., Sui, X. L., Wang, Z. B., Effect of Polytetrafluoroethylene (PTFE) in Current Collecting Layer on the Performance of Zinc-Air Battery, Progress in Natural Science: Materials International, Vol. 30, 2020, pp. 861–867.

[43] Leone, P., Santarelli, M., Asinari, P., Calì, M., and Borchiellini, R., Experimental Investigations of the Microscopic Features and Polarization Limiting Factors of Planar SOFCs with LSM and LSCF Cathodes, J. Power Sources, Vol. 177, 2008, pp. 111–122.

[44] Harting, K., Kunz, U., and Turek, T., Zinc-Air Batteries: Prospects and Challenges for Future Improvement, Zeitschrift für Physikalische Chemie, Vol. 226, 2012, pp. 151–166.

[45] Park, G. G., Sohn, Y. J., Yang, T. H., Yoon, Y. G., Lee, W. Y., and Kim, C. S., Effect of PTFE Contents in the Gas Diffusion Media on the Performance of PEMFC, J. Power Sources, Vol. 131, 2024, pp. 182–187.

[46] Daino, M. M., Kandlikar, S. G., 3D Phase-Differentiated GDL Microstructure Generation with Binder and PTFE Distributions, Int J. Hydrogen Energy, Vol. 37, 2012, pp. 5180–5189.

[47] Matsena, M. T., Mabuse, M., Tichapondwa, S. M., and Chirwa, E. M. N., Improved Performance and Cost Efficiency by Surface Area Optimization of Granular Activated Carbon in Air-Cathode Microbial Fuel Cell, Chemosphere, Vol. 281, 2021, pp. 130941.

[48] Barroso Bogeat, A., Understanding and Tuning the Electrical Conductivity of Activated Carbon: A State-of-the-Art Review. Critical Reviews in Solid State and Materials Sciences, Vol. 46, 2021, pp. 1–37.

[49] González, A., Goikolea, E., Barrena, J. A., and Mysyk, R., Review on Supercapacitors: Technologies and Materials. Renewable and Sustainable Energy Reviews, Vol. 58, 2016, pp. 1189–1206.

[50] Simon, P., Burke, A., Nanostructured Carbons: Double-Layer Capacitance and More, Electrochem Soc Interface, Vol. 17, 2008, pp. 38.

[51] Xu, C., Liu, X., Sumińska-Ebersoldt, O., Passerini, S., Al−Air Batteries for Seasonal/Annual Energy Storage: Progress Beyond Materials. Batter Supercaps, Vol. 7, 2024, pp. e202300590, doi:https://doi.org/10.1002/batt.202300590.